Article

Ligand-Assisted Reduction of Osmium Tetroxide with Molecular Hydrogen via a [3+2] Mechanism

Ahmad Dehestani, Wai Han Lam, David A. Hrovat, Ernest R. Davidson, Weston Thatcher Borden, and James M. Mayer

J. Am. Chem. Soc., **2005**, 127 (10), 3423-3432• DOI: 10.1021/ja043777r • Publication Date (Web): 12 February 2005

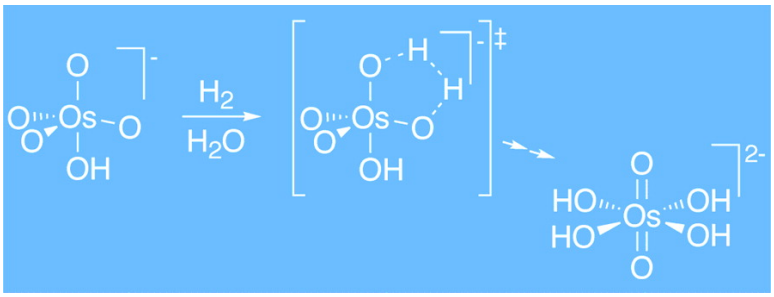

More About This Article

Additional resources and features associated with this article are available within the HTML version:

- Supporting Information
- Links to the 1 articles that cite this article, as of the time of this article download
- Access to high resolution figures
- Links to articles and content related to this article
- Copyright permission to reproduce figures and/or text from this article

View the Full Text HTML

J|A|C|S
ARTICLES
Published on Web 02/12/2005

Ligand-Assisted Reduction of Osmium Tetroxide with Molecular Hydrogen via a [3+2] Mechanism

Ahmad Dehestani, Wai Han Lam, David A. Hrovat, Ernest R. Davidson, Weston Thatcher Borden,* and James M. Mayer*

Contribution from the Department of Chemistry, University of Washington, Box 351700, Seattle, Washington 98195-1700

Received October 13, 2004; E-mail: borden@unt.edu; mayer@chem.washington.edu

Abstract: Osmium tetroxide is reduced by molecular hydrogen in the presence of ligands in both polar and nonpolar solvents. In $CHCl_3$ containing pyridine (py) or 1,10-phenanthroline (phen), OsO_4 is reduced by H_2 to the known Os(VI) dimers $L_2Os(O)_2(\mu\text{-}O)_2Os(O)_2L_2$ (L_2 = py_2, phen). However, in the absence of ligands in $CHCl_3$ and other nonpolar solvents, OsO_4 is unreactive toward H_2 over a week at ambient temperatures. In basic aqueous media, H_2 reduces $OsO_4(OH)_n^{n-}$ (n = 0, 1, 2) to the isolable Os(VI) complex, $OsO_2(OH)_4^{2-}$, at rates close to that found in py/$CHCl_3$. Depending on the pH, the aqueous reactions are exergonic by $\Delta G = -20$ to -27 kcal mol^{-1}, based on electrochemical data. The second-order rate constants for the aqueous reactions are larger as the number of coordinated hydroxide ligands increases, $k_{OsO_4} = 1.6(2) \times 10^{-2}$ M^{-1} s^{-1} < $k_{OsO_4(OH)^-} = 3.8(4) \times 10^{-2}$ M^{-1} s^{-1} < $k_{OsO_4(OH)_2^{2-}} = 3.8(4) \times 10^{-1}$ M^{-1} s^{-1}. The observation of primary deuterium kinetic isotope effects, $k_{H_2}/k_{D_2} = 3.1(3)$ for OsO_4 and 3.6(4) for $OsO_4(OH)^-$, indicates that the rate-determining step in each case involves H−H bond cleavage. Density functional calculations and thermochemical arguments favor a concerted [3+2] addition of H_2 across two oxo groups of $OsO_4(L)_n$ and argue against H• or H^- abstraction from H_2 or [2+2] addition of H_2 across one Os=O bond. The [3+2] mechanism is analogous to that of alkene addition to $OsO_4(L)_n$ to form diolates, for which acceleration by added ligands has been extensively documented. The observation that ligands also accelerate H_2 addition to $OsO_4(L)_n$ highlights the analogy between these two reactions.

Introduction

The activation of molecular hydrogen (dihydrogen) by transition metal compounds is a fundamental reaction in both homogeneous and heterogeneous chemistry.[1] The most common and most studied examples involve oxidative addition of H_2 to low-valent metal centers or H_2 addition to a metal surface (Scheme 1a). H_2 is also widely used as a reductant for high-valent compounds such as metal oxides, for instance, in the activation of calcined precatalysts.[1d,e] One of the few heterogeneous reactions of H_2 with an oxide surface that has been studied in detail is that with zinc oxide, an important step in the conversion of CO + H_2 (syn gas) to methanol. H_2 is thought to add across a Zn−O bond in a [2+2] mechanism to give a Zn(H)−OH fragment.[2] This [2+2] mechanism[3] (Scheme 1b) has been termed σ-bond metathesis when the original M−X bond is cleaved. Homogeneous examples of [2+2] reactions of H_2 include additions to the multiple bonds in $Cp^*_2Zr(=O)py$, $Cp^*_2Ti=S$, $Cp'_2Ti=NR$, and $(^tBu_3SiNH)_2(THF)Zr=NSi^tBu_3$, and to ruthenium amides (Ru=NHR) to give $Ru(H)NH_2R$.[4−8] Both the oxidative addition and the [2+2] pathways can involve metal−dihydrogen complexes.[1f,5,8]

Scheme 1. Pathways for Concerted Addition of H_2 to a Metal Complex

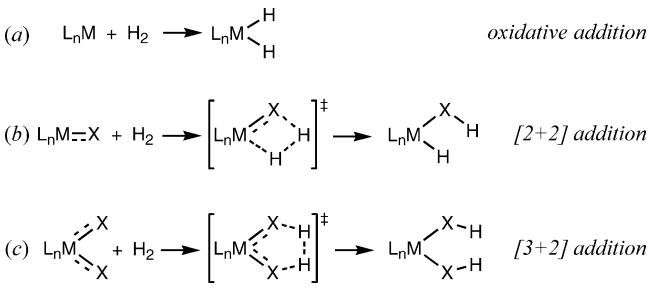

(1) (a) Collman, J. P.; Hegedus, L. S.; Norton, J. R.; Finke, R. G. *Principles of Organometallic Metal Chemistry*; University Science Books: Mill Valley, CA, 1987. (b) Crabtree, R. H. *The Organometallic Chemistry of Transition Metals*; Wiley: New York, 1988. (c) Parshall, G. W. *Homogeneous Catalysis*; Wiley: New York, 1980. (d) Thomas, J. M.; Thomas, W. J. *Principles and Practice of Heterogeneous Catalysis*; Wiley-VCH: New York, 1997. (e) Kung, H. H. *Transition Metal Oxides: Surface Chemistry and Catalysis*; Elsevier: New York, 1989. (f) Kubas, G. J. *Metal dihydrogen and σ-bond complexes*; Kluwer Academic: New York, 2001.
(2) Anderson, A. B.; Nichols, J. A. *J. Am. Chem. Soc.* **1986**, *108*, 4742.
(3) For an introduction to [2+2] reactions of metal-oxo complexes, see: Pilato, R. S.; Housmekerides, C. E.; Jernakoff, P.; Rubin, D.; Geoffroy, G. L. *Organometallics* **1990**, *9*, 2333−2341.
(4) (a) Howard, W. A.; Waters, M.; Parkin, G. *J. Am. Chem. Soc.* **1993**, *115*, 4917−8. (b) Howard, W. A.; Trnka, T. M.; Waters, M.; Parkin, G. *J. Organomet. Chem.* **1997**, *528*, 95−121.
(5) (a) Sweeney, Z. K.; Polse, J. L.; Andersen, R. A.; Bergman, R. G.; Kubinec, M. G. *J. Am. Chem. Soc.* **1997**, *119*, 4543. (b) Sweeney, Z. K.; Polse, J. L.; Andersen, R. A.; Bergman, R. G.; Kubinec, M. G. *Organometallics* **1999**, *18*, 5502−5510.
(6) Hanna, T. E.; Keresztes, I.; Lobkovsky, E.; Bernskoetter, W. H.; Chirik, P. J. *Organometallics* **2004**, *23*, 3448−3458; Cp′ = C_5H_3-1,3-$(SiMe_3)_2$; R = $SiMe_3$, 2,4,6-$Me_3C_6H_2$.
(7) Schaller, C. P.; Cummins, C. C.; Wolczanski, P. T. *J. Am. Chem. Soc.* **1996**, *118*, 591−611.
(8) Abdur-Rashid, K.; Clapham, S. E.; Hadzovic, A.; Harvey, J. N.; Lough, A. J.; Morris, R. H. *J. Am. Chem. Soc.* **2002**, *124*, 15104.

10.1021/ja043777r CCC: $30.25

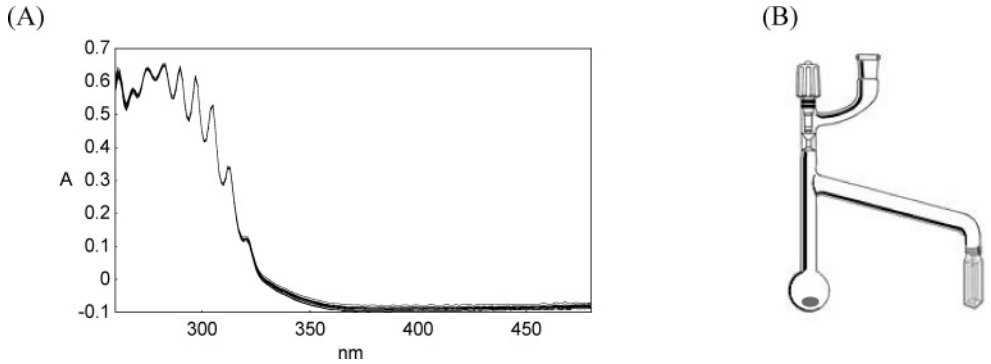

Figure 1. (A) Overlay of 39 spectra of 0.45 mM OsO_4 in CCl_4 under 1.03 atm of H_2 over 168 h at 297 K. (B) Drawing of the apparatus used for optical monitoring of reactions, consisting of a Teflon stopcock and 24/40 ground glass joint attached to a 25 mL flask and a 3.5 mL quartz cuvette.

There are only a small number of studies of homogeneous hydrogenations of metal oxo compounds.[4a,9−11] The H_2 reduction of permanganate solutions to solid manganese dioxide has received the most attention, starting as far back as 1911.[9−11] A mechanistic study in aqueous solutions by Webster and Halpern in 1957 concluded that Mn(V) was a likely intermediate.[10]

A recent stimulating experimental and computational paper by Collman, Strassner, et al. described hydrogenations of MnO_4^- to solid MnO_2 in both H_2O and C_6H_5Cl solvents, and the related reduction of RuO_4 to RuO_2 in CCl_4.[11] They concluded that Mn(V) is formed by addition of H_2 to two oxo groups via a [3+2] transition state (Scheme 1c). Net H_2 addition to the two imido ligands of $Cp^*_2U(=NPh)_2$ to give $Cp^*_2U(NHPh)_2$ has also been described.[12]

The [3+2] mechanism is an interesting contrast to the oxidative addition and [2+2] pathways in that hydrogen binds only to the ligands X, without M−H bond formation. The [3+2] path should in general be favored by oxidizing metal centers, because the addition of both hydrogens to the ligands results in a formal two-electron reduction of the metal. The [2+2] mechanism does not involve a metal redox change, and oxidative addition, as the name suggests, is a formal oxidation of M.

Collman et al. reported that 1 atm of H_2 does not reduce OsO_4, $MeReO_3$, or $KReO_4$ over several days at room temperature in either CCl_4 or H_2O.[11] It is known, from both experimental and computational studies, that OsO_4 oxidizes olefins by a [3+2] mechanism[13] and that such oxidations are accelerated by ligation of tertiary amines to the osmium (to form $OsO_4(L)_n$).[14] We suspected that a [3+2] reaction of OsO_4 with H_2 would similarly be facilitated by ligand binding. We were also led to this hypothesis through our studies of a reactive osmium(VIII) complex with a hydrotris(1-pyrazolyl)borate (Tp) ligand.[15]

We report here that H_2 readily reduces $OsO_4(L)_n$, and we present kinetic, mechanistic, and computational studies of these reactions. $OsO_4(L)_n$ complexes are particularly attractive for mechanistic studies because they undergo two-electron reductions to well-characterized osmium(VI) products (reductions of MnO_4^- and RuO_4 yield insoluble metal dioxides, MO_2). The stoichiometric simplicity of the aqueous $OsO_4 + H_2$ reactions allows the determination of the thermochemical driving force from electrochemical data. Reduction of OsO_4 by H_2 is accelerated by added ligands, in analogy to the [3+2] addition of OsO_4 to alkenes. DFT calculations predict the acceleration of the reaction by osmium ligation, and the calculations indicate that the [3+2] pathway is highly favored.

Results

I. Reactions of OsO_4·L with H_2 in Organic Solvents. Solutions of OsO_4 in $CHCl_3$, CCl_4, and *n*-hexane are unchanged after a week under 1 atm of H_2 at ambient temperatures, as indicated by a lack of change in the UV−vis spectra (Figure 1A shows 39 overlaid spectra). A control experiment, done under 1 atm of air, also showed no change. These experiments and most of those described below were performed in the apparatus shown in Figure 1B. Solutions were freeze−pump−thaw degassed in the flask prior to H_2 addition and were stirred throughout the reaction. Prior to acquiring each spectrum (ca. every 15 min for the kinetic studies described below), the whole apparatus was shaken to promote equilibration of dissolved and gaseous H_2. Initial experiments showed that this equilibration was slow on the time scale of the reaction for an unstirred solution in a cuvette directly attached to a Teflon stopcock.

In $CHCl_3$ in the presence of pyridine (24:1), OsO_4 reacts with 1 atm of H_2 over the course of 16 h. The solution, which is initially yellow due to rapid formation of the pyridine adduct $OsO_4(py)$,[16] gradually turns colorless, and a bright golden-brown precipitate is formed. The precipitate was identified as the osmium(VI)-oxo-pyridine dimer $Os_2O_6(py)_4$ by comparison of its IR and ^1H NMR spectra with those described in the literature and with spectra of an authentic sample.[17] A balanced equation for this reaction is shown in eq 1.

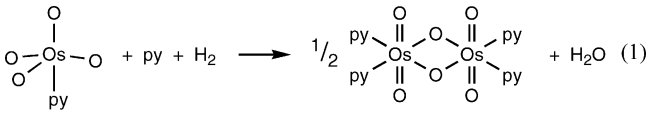

OsO_4(phen), formed from OsO_4 and excess 1,10-phenanthroline in chloroform,[18] reacts similarly with H_2. The nature of

(9) Just, G; Kauko, Y. *Z. Phys. Chem.* **1911**, *76*, 601.
(10) (a) Halpern, J. *Adv. Catal.* **1957**, *9*, 302. (b) Webster, A. H.; Halpern, J. *Trans. Faraday Soc.* **1957**, *53*, 51.
(11) Collman, J. P.; Slaughter, L. M.; Eberspacher, T. S.; Strassner, T.; Brauman, J. I. *Inorg. Chem.* **2001**, *40*, 6272.
(12) Arney, D. S. J.; Burns, C. J. *J. Am. Chem. Soc.* **1995**, *117*, 9448−9460.
(13) (a) Delmonte, A. J.; Haller, J.; Houk, K. N.; Sharpless, K. B.; Singleton, D. A.; Strassner, T.; Thomas, A. A. *J. Am. Chem. Soc.* **1997**, *119*, 9907 and references therein. (b) Dapprich, S.; Ujaque, G.; Feliu, M.; Lledós, A.; Musaev, D. G.; Morokuma, K. *J. Am. Chem. Soc.* **1996**, *118*, 11660. (c) Pidum, U.; Boehme, C.; Frenking, G. *Angew. Chem.* **1996**, *108*, 3008. Deubel, D. V.; Frenking, G. *Acc. Chem. Res.* **2003**, *36*, 645−651. (d) Torrent, M.; Deng, L.; Duran, M.; Sola, M.; Ziegler, T. *Organometallics* **1997**, *16*, 13. (e) Strassner, T. *Adv. Phys. Org. Chem.* **2003**, *38*, 131−160.
(14) (a) Kolb, H. C.; Van Nieuwenhze, M. S.; Sharpless, K. B. *Chem. Rev.* **1994**, *94*, 2483. (b) Reference 13.
(15) Dehestani, A.; Wu, A.; Hrovat, D. A.; Kaminsky, W.; Mayer, J. M., manuscript in preparation.

the $Os_2O_6(phen)_2$ product was again confirmed by comparison with an authentic sample.[17b] In this system, the monomeric osmium(VI) bis(hydroxide) complex $OsO_2(OH)_2(phen)$ and its dimerization to $Os_2O_6(phen)_2$ + water have been described.[17b,18] Most likely, this bis(hydroxide) complex is an intermediate in the reaction (eq 2) but is not observed because its dimerization is faster than the reaction of $OsO_4(phen)$ with H_2.[17,18] Reaction 1 probably also involves a bis(hydroxide) intermediate.

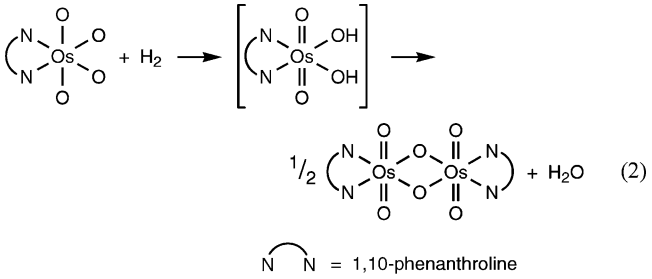

The kinetics of the reaction of $OsO_4(py)$ with H_2 were followed in $CHCl_3$ solution (1.6 mM OsO_4, 0.25 M py). There was a general increase in optical absorption over 15 h (Figure S1, Supporting Information), while a control experiment with the same solution but without H_2 showed no decay of the characteristic spectrum of $OsO_4(py)$ (Figure S2). Unfortunately, much of the increased absorption is due to the formation of the $Os_2O_6(py)_4$ precipitate. Consequently, only a rough estimate of the second-order rate constant was possible, $k_1 = 2.4(8) \times 10^{-2}$ M^{-1} s^{-1} (the reaction presumed to be first order in $[OsO_4]$ and in $[H_2]$[19]). A similar rate constant was obtained when *n*-hexane was used in place of $CHCl_3$ as the solvent.

II. Reactions of OsO_4 with H_2 in Water. A. Speciation of OsO_4 in Water. The studies that have examined the speciation of OsO_4 as a function of pH are in general concurrence if not in quantitative agreement.[20] In alkaline solutions, OsO_4 expands its coordination number to form $OsO_4(OH)^-$ and *cis*-$OsO_4(OH)_2^{2-}$.[20d,e] X-ray crystal structures have been reported for OsO_4,[21] *cis*-$OsO_4(OH)_2^{2-}$,[22] and a number of five-coordinate OsO_4·L derivatives (L = a nitrogen donor)[23] although not for a salt of $OsO_4(OH)^-$. *cis*-$OsO_4(OH)_2^{2-}$ is formed only at pH > 14 ($pK_{a2} = 14.4$), and under these conditions it spontaneously reduces to osmate, *trans*-$Os^{VI}O_2(OH)_4^{2-}$.[20,24] Osmate is commercially available as the potassium salt and is the dominant osmium(VI) species in aqueous solutions above pH 5.[20]

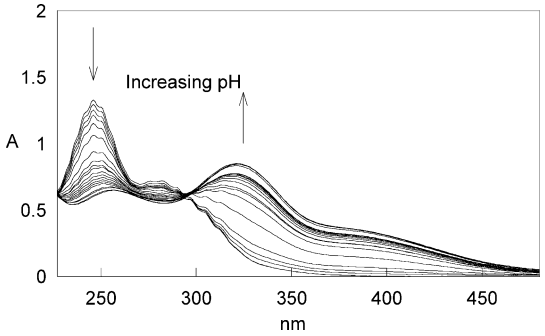

Figure 2. Spectra of 0.43 mM OsO_4 in 0.170 M phosphate buffer as a function of pH from 8.4 to 13.0. Spectra are virtually unchanged from pH 4.3−8.4.

We have examined OsO_4 in aqueous phosphate buffer (typically 0.17 M). At neutral pH, the predominant species appears to be the unligated tetrahedral OsO_4 based on UV−visible spectra. The spectra are similar to those of gas-phase OsO_4 and of OsO_4 solutions in noncoordinating media such as CCl_4 (Figure 1A).[25] The spectra display structured absorptions indicative of a high-symmetry species with a low density of vibrational states. Spectra of OsO_4 in buffered Millipore water (pH = 4.5−9.2) also show vibrational structure, although the individual lines are broader than those in the spectra taken in CCl_4.

Raising the pH causes a substantial change in the optical spectrum of OsO_4 as $OsO_4(OH)^-$ is formed (Figure 2). Analysis of the spectra (Figure S3) shows that one hydroxide binds to OsO_4 with $K = 130$ M^{-1} (eq 3), implying $K_a = 1.3 \times 10^{-12}$ M

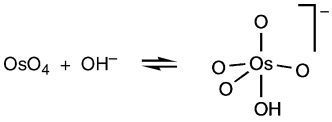

($pK_a = 11.9$). This is close to the literature value of 6.3×10^{-13} M measured in the absence of buffer.[20f,g] The extinction coefficients for OsO_4 ($\epsilon_{250} = 3020$ M^{-1} cm^{-1}, $\epsilon_{325} = 370$ M^{-1} cm^{-1}) and for $OsO_4(OH)^-$ ($\epsilon_{250} = 1470$ M^{-1} cm^{-1}, $\epsilon_{325} = 1950$ M^{-1} cm^{-1}) in buffered solutions are within the error of the literature values in unbuffered solutions ($\epsilon_{250} = 3100$ M^{-1} cm^{-1}, $\epsilon_{325} = 380$ M^{-1} cm^{-1} and $\epsilon_{250} = 1480$ M^{-1} cm^{-1}, $\epsilon_{325} = 2000$ M^{-1} cm^{-1}).[20f] These data show that the phosphate buffer is not binding to OsO_4.

B. Reactions of OsO_4 with H_2 in Water. Solutions of OsO_4 in phosphate buffer at pH ≤ 13 show no change by UV−visible spectroscopy over days at ambient temperatures. Upon exposure to 1 atm of H_2, these light yellow solutions turn pink. The optical spectra indicate quantitative formation of $OsO_2(OH)_4^{2-}$ (eq 4), by comparison with literature values[20e] and with the spectrum of a commercial sample of $K_2OsO_2(OH)_4$ at the same pH and buffer concentration.

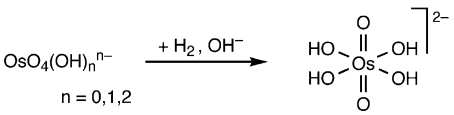

(16) Griffith, W. P.; Rosetti, R. J. *J. Chem. Soc., Dalton Trans.* **1972**, *53*, 1449.
(17) (a) El-Hendawy, A. M.; Griffith, W. P.; Taha, F. I.; Moussa, M. N. *J. Chem. Soc., Dalton Trans.* **1989**, 901. (b) Galas, A. M. R.; Hursthouse, M. B.; Behrman, E. J.; Midden, W. R.; Green, G.; Griffith, W. P. *Transition Met. Chem. (London)* **1981**, *6*, 194.
(18) Chang, C.-H.; Midden, W. R.; Deetz, J. S.; Behram, E. J. *Inorg. Chem.* **1979**, *18*, 1364.
(19) The concentration of H_2 was calculated from data in: *IUPAC Solubility Data Series: Hydrogen and Deuterium*; Young, C. L., Ed.; Pergamon Press: New York, 1981; p 5.
(20) (a) Richens, D. T. *The Chemistry of Aqua Ions*; John Wiley and Sons: New York, 1997; p 427. (b) Baes, C. F., Jr.; Mesmer, R. E. *The Hydrolysis of Cations*; Wiley: New York, 1976. (c) Pourbaix, M. *Atlas of Electrochemical Equilibria in Aqueous Solutions*; Pergamon Press: New York, 1966; p 365. (d) Ivan-Emin, N. N.; Nevskaya, N. A.; Nevskii, N. N.; Izmailovich, A. S. *Russ. J. Inorg. Chem. (Engl. Transl.)* **1984**, *29*, 710. (e) Jewiss, H. C.; Levason, W.; Tajik, M.; Webster, M.; Walker, N. P. C. *J. Chem. Soc., Dalton Trans.* **1985**, 199. (f) Galbács, Z. M.; Zsednai, A.; Csányi, L. J. *Transition Met. Chem. (London)* **1983**, *8*, 328. (g) Bavay, J. C.; Nowogrocki, G.; Tridot, G. *Bull. Soc. Chim. Fr.* **1976**, 2026.
(21) Krebs, B.; Hasse, K. D. *Acta Crystallogr., Sect. B* **1976**, *32*, 1334.
(22) (a) Nevskii, N. N.; Ivan-Emin, B.; Nevskaya, O. N. A.; Belov, N. V. *Dokl. Akad. Nauk SSSR* **1983**, *226*, 245. The cis isomer of $OsO_4(OH)_2^{2-}$ allows the maximum number of d orbitals to be available for Os-oxo π bonding: Lin, Z. Y.; Hall, M. B. *Coord. Chem. Rev.* **1993**, *123*, 149. (b) Richens, D. T. *The Chemistry of Aqua Ions*; John Wiley and Sons: New York, 1997; p 427.
(23) Nelson, D. W.; Gypser, A.; Ho, P. T.; Kolb, H. C.; Kondo, T.; Kwong, H.-L.; McGrath, A.; Rubin, E. A.; Norbby, P.-O.; Gable, K. P.; Sharpless, K. B. *J. Am. Chem. Soc.* **1997**, *119*, 1840.

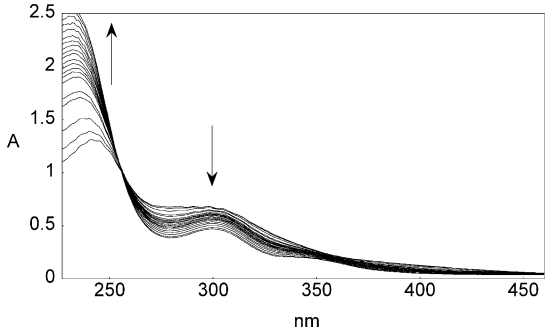

Figure 3. Spectra of the reaction of OsO_4 (0.38 mM) in 0.17 M phosphate buffer under 1.03 atm H_2 taken over 34 h.

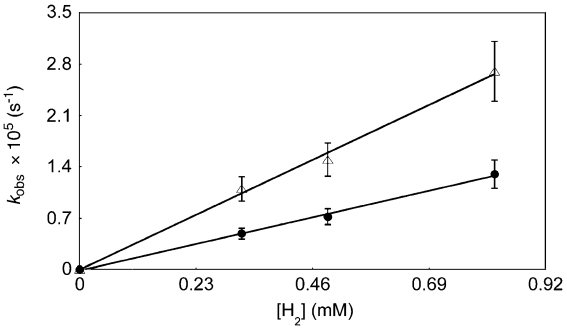

Figure 4. Plot of the pseudo-first-order rate constant, k_{obs}, versus $[H_2]$ at 298 K for reaction of ~0.40 mM $[OsO_4]$ plus excess H_2 (g) in 0.17 M phosphate buffer at pH 9.22 (●) and 12.31 (△).

The kinetics of reactions of OsO_4 with H_2 at various pH values were monitored by optical spectroscopy (Figure 3) using the cell and procedure described above. The volume of the apparatus and the stirring and frequent shaking ensure constant $[H_2]$ over the course of the reaction. Reactions were typically run at ~0.40 mM OsO_4 in 0.17 M phosphate buffer, adjusted to the desired pH by addition of NaOH prior to addition of OsO_4.

Global analyses of spectra from 230 to 600 nm over 2−3 half-lives, using SPECFIT,[26] indicate that the reactions follow first-order kinetics (A→B). Varying the OsO_4 concentration by a factor of 2 (from 0.21 to 0.43 mM) at pH 9.22 gave the same pseudo-first-order rate constants, k_{obs}, within experimental error. The k_{obs} values vary linearly with H_2 concentration from 0.36 to 0.82 mM (0.45−1.03 atm), at both pH 9.22 and pH 12.31 (Figure 4). Thus, the reactions are first order in both H_2 and $[OsO_4(OH)_n]^{n-}$. The H_2 concentrations were calculated from literature solubility data for the same pH and buffer ionic strength (different buffers have only a minimal effect, ~±5%, on the H_2 solubility).[19] Varying the buffer concentration from 0 to 0.300 M gave only a 12% random variation in the observed rates, indicating that phosphate is not kinetically important. Eyring analyses of rate constants from 8 to 68 °C (Figure S4) gave $\Delta H^{\ddagger} = 13.2(2)$ kcal mol^{-1} and $\Delta S^{\ddagger} = -22.3(3)$ cal mol^{-1} K^{-1} at pH 9.22 and $\Delta H^{\ddagger} = 12.9(2)$ kcal mol^{-1} and $\Delta S^{\ddagger} = -21.9(3)$ cal mol^{-1} K^{-1} at pH 12.31.

The kinetics of OsO_4 reduction have been examined at pH values from 4.3 to 14.6 (Table 1). At pH's other than 9.22 and 12.31, and for the reactions with D_2 gas, measurements were made only at 1 atm of H_2 or D_2, and k_2 was taken to be k_{obs}/$[H_2]$. The reactions with D_2 indicate kinetic isotope effects, k_{H_2}/k_{D_2}, of 3.1(3) at pH 9.22 and 3.7(4) at pH 12.31. In 4 M NaOH (nominally pH 14.6), $OsO_4(OH)_2^{2-}$ decomposes to $OsO_2(OH)_4^{2-}$ with $k_{obs} = 1.1(1) \times 10^{-4}$ s^{-1}. Upon addition of H_2 (1 atm, 0.8 mM), k_{obs} increases to $4.1(4) \times 10^{-4}$ s^{-1}. Assuming that the increase is due to a bimolecular reaction of H_2 with Os^{VIII}, k_2 at this pH is $3.8(4) \times 10^{-1}$ M^{-1} s^{-1}.

Table 1. Rate Constants for $OsO_4(OH)_n^{n-}$ Reduction by H_2 or D_2 (24 °C, $n = 0, 1, 2$)[a]

pH	k_2 (M^{-1} s^{-1})
4.27	$2.3(2) \times 10^{-3}$
4.32	$2.4(2) \times 10^{-3}$
7.00	$6.6(8) \times 10^{-3}$
8.50	$1.5(3) \times 10^{-2}$
9.22	$1.6(2) \times 10^{-2}$
9.22	$5.2(7) \times 10^{-3}$ (D_2)
9.34	$1.8(2) \times 10^{-2}$
10.64	$1.7(2) \times 10^{-2}$
10.75	$1.8(3) \times 10^{-2}$
11.36	$2.0(2) \times 10^{-2}$
11.80	$2.3(2) \times 10^{-2}$
12.10	$2.7(3) \times 10^{-2}$
12.21	$3.3(4) \times 10^{-2}$
12.31	$3.3(4) \times 10^{-2}$
12.31	$9.0(8) \times 10^{-3}$ (D_2)
12.35	$3.5(5) \times 10^{-2}$
12.50	$3.8(4) \times 10^{-2}$
14.60[b]	$3.8(4) \times 10^{-1}$ [b]

[a] Total [Os] typically ~0.4 mM (varied at pH 12.31 from 0.21 to 0.68 mM); $[H_2]$ or $[D_2]$ typically ~0.80 mM (at pH 9.22 and 12.31 varied from ~0.34 to ~0.83 mM); phosphate buffer concentration 0−0.3 M (most often 0.17 M). For a complete list of rate constants and conditions, see Table S1. [b] 4 M NaOH; k_2 corrected for the decomposition of *cis*-$Os(O)_4(OH)_2^{2-}$.

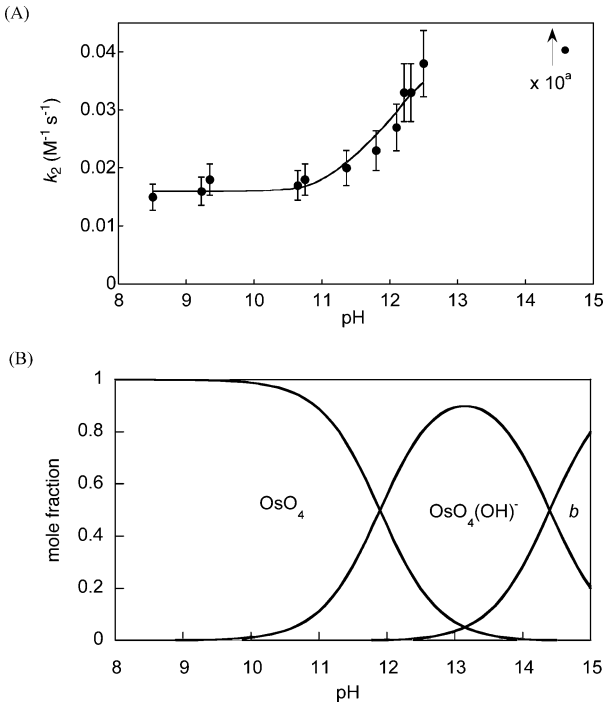

Figure 5. (A) Plot of second-order rate constants, k_2, versus pH. Below pH 10, the osmium is predominantly OsO_4. The line represents the best fit to eq 6. [a]The second-order rate constant of 0.38 M^{-1} s^{-1} at pH 14.60 is reduced 10 times to fit on the plot. (B) Speciation curve of $OsO_4(OH)_n^{n-}$ where *b* represents $OsO_4(OH)_2^{2-}$.

The bimolecular rate constants increase with rising pH (Figure 5A). For comparison, the speciation of OsO_4 with pH is plotted on the same pH scale in Figure 5B. Between pH 8 and 13, the

(24) Norkus, K. P.; Rozovsky, G. I.; Yankauskas, Y. Y. *Zh. Anal. Khim.* **1971**, *26*, 1827.
(25) Wells, E. J.; Jordan, A. D.; Alderdice, D. S.; Ross, I. G. *Aust. J. Chem.* **1967**, *20*, 2315.
(26) SPECFIT (Spectrum Software Associates, Marlborough, MA).

Table 2. Calculated Energies (kcal mol^{-1}) and Entropies (cal K^{-1} mol^{-1}) Relative to $OsO_4(L) + H_2$[a]

	ΔE[b]	ΔH	ΔS	ΔG
	$OsO_4 + H_2$			
[2+2] transition state	58.6	58.7	−23.9	65.9
$HOs(O)_3(OH)$	17.0	20.9	−21.8	27.5
[3+2] transition state	18.3	18.8	−26.7	26.8
$Os(O)_2(OH)_2$[c]	−41.2	−35.0	−22.2	−28.3
	$OsO_4(OH)^- + H_2$			
[2+2] transition state	44.5	44.6	−31.7	54.1
$HOs(O)_3(OH)_2^-$	2.5	6.4	−28.6	15.0
[3+2] transition state	10.3	10.6	−29.9	19.5
$Os(O)_2(OH)_3^-$[c]	−57.2	−51.1	−26.2	−43.3
	$OsO_4(NH_3) + H_2$			
[2+2] transition state	56.5	56.6	−30.2	65.6
$HOs(O)_3(OH)(NH_3)$	8.8	13.0	−29.4	21.8
[3+2] transition state	14.4	14.9	−28.3	23.3
$Os(O)_2(OH)_2(NH_3)$[c]	−51.8	−45.3	−28.6	−36.8

[a] At 298 K. [b] Electronic energies. [c] Energies of the most stable conformer (Figure 8); other conformations have different orientations of the H atoms in the two formed hydroxyl groups.[29]

dominant species in solution are OsO_4 and $OsO_4(OH)^-$, indicating the rate law in eq 6. Using the K_a derived above for $OsO_4 + 2\ H_2O \rightleftharpoons OsO_4(OH)^- + H_3O^+$ yields eq 7. Equation 7 provides a good fit to the rate constants from pH 8.5 to 12.5, as indicated by the line in Figure 5A.

$$\frac{d[Os^{VIII}]}{dt} = k_2[Os^{VIII}][H_2] = k_{OsO_4}[OsO_4][H_2] + k_{OsO_4OH^-}[OsO_4(OH)^-][H_2] \quad (6)$$

$$\frac{d[Os^{VIII}]}{dt} = [Os^{VIII}][H_2]\left\{\frac{k_{OsO_4}}{1 + K_a/[H^+]} + \frac{k_{OsO_4OH^-}}{1 + [H^+]/K_a}\right\} \quad (7)$$

It should be noted that the rate constants decrease by a factor of 6.5 on decreasing the pH from pH 8.5 and 4.3 (Table 1; not shown in Figure 5). The origin of this rate retardation at lower pH is not known, but may be due to the formation of solid OsO_2 instead of $[Os(O)_2(OH)_4]^{2-}$.[27]

As indicated in Figure 5B, at pH 9.22 aqueous Os^{VIII} is >99% OsO_4, so the rate constants, isotope effect, and activation parameters measured at that pH correspond to reactions of OsO_4. At pH 12.31, solutions are 28% OsO_4 and 72% $OsO_4(OH)^-$. After correcting for this speciation, the reaction of $OsO_4(OH)^-$ with H_2 has $k_{OsO_4OH^-} = 3.8(4) \times 10^{-2}$ M^{-1} s^{-1}, an isotope effect $k_{H_2}/k_{D_2} = 3.6(4)$, and activation parameters $\Delta H^{\ddagger} = 12.8(2)$ kcal mol^{-1} and $\Delta S^{\ddagger} = -21.8(2)$ cal mol^{-1} K^{-1}.[28] The reaction of H_2 with $OsO_4(OH)^-$ is roughly 2.4 times as fast as that with OsO_4; the activation parameters are the same within experimental error. $OsO_4(OH)_2^{2-}$ reacts with H_2 an order of magnitude faster than $OsO_4(OH)^-$.

Computational Studies. The reactions of OsO_4, $OsO_4(OH)^-$, and $OsO_4(NH_3)$ with H_2 have been studied at the B3LYP level of density functional theory (DFT). The details of the methodology used are described at the end of the experimental section. Computed gas-phase reaction energies, enthalpies, and free energies are shown in Table 2.

(27) Permanganate reactions are often affected by the formation of solid MnO_2, with MnO_4^- apparently absorbing onto MnO_2 and being activated: cf., Lee, D. G.; Perez-Benito, J. F. *Can. J. Chem.* **1985**, *63*, 1275−1279 and references therein.

(28) The derivation of activation parameters for $OsO_4(OH)^-$ assumes that the 72/28 ratio of $OsO_4(OH)^-/OsO_4$ in reaction solutions at 297 K does not change significantly with temperature.

Scheme 2. Addition of H_2 and OH^- to OsO_4

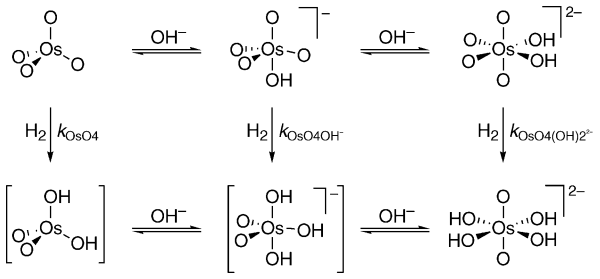

All of the reactions are predicted to be exergonic, with gas-phase free energies from −28.3 kcal mol^{-1} for $OsO_4 + H_2 \rightarrow OsO_2(OH)_2$ to −43.3 kcal mol^{-1} for $OsO_4(OH)^- + H_2 \rightarrow OsO_2(OH)_3^-$. These values are in the range of solution values determined from aqueous electrochemical measurements (~ -25 kcal mol^{-1}, see below). Closer agreement should not be expected, because the experimental values refer to the formation of aqueous $OsO_2(OH)_4^{2-}$.

Gas-phase transition structures were located for the addition of H_2 to each of the three osmium species by both [2+2] and [3+2] pathways. As discussed below, addition of OH^- and NH_3 to OsO_4 is predicted to accelerate the reaction with H_2 and make both the [2+2] and the [3+2] pathways more favorable, kinetically as well as thermodynamically. However, the [2+2] reaction is computed to be very endergonic for OsO_4, $OsO_4(OH)^-$, and $OsO_4(NH_3)$, so only the [3+2] reaction is predicted to occur.

Discussion

Dihydrogen readily reduces $OsO_4(L)_n$ species at room temperature. In aqueous solutions, reductions of OsO_4 and $OsO_4(OH)^-$ both exhibit activation parameters of $\Delta H^{\ddagger} = \sim 13$ kcal mol^{-1} and $\Delta S^{\ddagger} = \sim -22$ cal mol^{-1} K^{-1}. Overall conversion of OsO_4 and H_2 to the product, $OsO_2(OH)_4^{2-}$, requires the binding of two hydroxide ions, either prior to or after the H_2 activation step (Scheme 2). We begin our discussion with the overall thermochemistry of H_2 addition, then proceed to mechanistic discussions, based on experimental and computational results.

I. Thermochemistry of H_2 Addition. The free energy of reaction for aqueous OsO_4 and H_2 as a function of pH can be derived from the aqueous redox potentials. These are summarized in the partial Pourbaix or *E*/pH diagram in Figure 6 and in the equations in Scheme 3 (adapted from ref 20c and corrected for the slightly different pK_a values found here). In

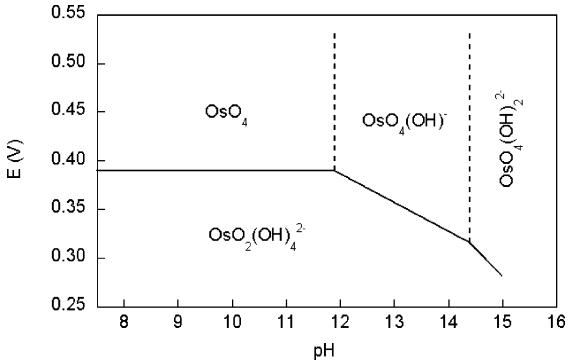

Figure 6. Partial Pourbaix (*E*/pH) diagram for OsO_4 (1 M concentrations, *E* vs NHE).[20c]

Scheme 3. Aqueous Thermochemistry of $OsO_4 + H_2$

$$OsO_4 + 2\,e^- + 2\,H_2O \rightleftharpoons OsO_2(OH)_4^{2-} \qquad E = 0.39 \qquad (8)$$

$$OsO_4(OH)^- + 2\,e^- + H_2O + H^+ \rightleftharpoons OsO_2(OH)_4^{2-} \qquad E = 0.74 - 0.0295\ pH \qquad (9)$$

$$OsO_4(OH)_2^{2-} + 2\,e^- + 2\,H^+ \rightleftharpoons OsO_2(OH)_4^{2-} \qquad E = 1.17 - 0.0591\ pH \qquad (10)$$

$$H_2 \rightleftharpoons 2\,H^+ + 2\,e^- \qquad E = 0 - 0.0591\ pH \qquad (11)$$

$$OsO_4 + H_2 + 2\,H_2O \rightleftharpoons OsO_2(OH)_4^{2-} + 2\,H^+ \qquad \Delta G^\circ = 0.93\ V = -22\ kcal\ mol^{-1}\ at\ pH\ 9.2 \qquad (12)$$

$$OsO_4(OH)^- + H_2 + H_2O \rightleftharpoons OsO_2(OH)_4^{2-} + H^+ \qquad \Delta G^\circ = 1.10\ V = -25\ kcal\ mol^{-1}\ at\ pH\ 12.3 \qquad (13)$$

$$OsO_4(OH)_2^{2-} + H_2 \rightleftharpoons OsO_2(OH)_4^{2-} \qquad \Delta G^\circ = 1.17\ V = -27\ kcal\ mol^{-1} \qquad (14)$$

Scheme 4. OsO−H Bond Dissociation Free Energies[30]

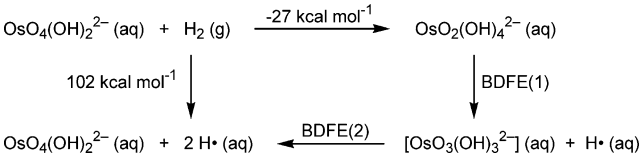

Figure 6, the vertical dashed lines indicate the pK_a values that separate the regions where OsO_4, $OsO_4(OH)^-$, and $OsO_4(OH)_2^{2-}$ are the predominant species (Figure 5B), and the horizontal lines describe the redox potentials versus the normal hydrogen electrode (NHE) for the half reactions in eqs 8−10. The uncertainties in E are estimated to be ±40 mV (±1 kcal mol^{-1}). Combining these half-reactions with the pH-dependent H^+/H_2 potential (eq 11) gives $\Delta G°$ for reactions of H_2 with aqueous OsO_4 at any pH (eqs 12−14). In these equations, $\Delta G°$ is for all species at standard state except for H^+.

The free energy of eq 14, which includes only osmium species and H_2, can be used in the thermochemical cycle in Scheme 4 to show that the sum of the aqueous bond dissociation free energies (BDFEs) of the two O−H bonds formed is 102 + 27 = 129 kcal mol^{-1}.[30] The unobserved Os(VII) intermediate, $[OsO_3(OH)_3^{2-}]$, is unstable with respect to disproportionation to Os(VI) and Os(VIII),[31] so BDFE(1) should be greater than BDFE(2). This implies that BDFE(2) is less than 65 kcal mol^{-1}. This value is also a reasonable upper bound for the bond dissociation enthalpy (BDE, the more common measure of bond strength).[32] Preliminary calculations indicate that in gas-phase $OsO_2(OH)_2$(L) and $OsO_3(OH)$(L), the OsO−H BDEs vary from 50 to 92 kcal mol^{-1} depending on the oxidation state of the osmium and its ligands.[33]

II. Reaction Mechanism. The bimolecular kinetics, the negative activation entropies, and the primary KIEs, k_{H_2}/k_{D_2} = 3.1(3) for OsO_4 and 3.6(4) for $OsO_4(OH)^-$, all indicate a rate-determining step involving cleavage of the H−H bond upon interaction with an Os^{VIII} species. Similar k_{H_2}/k_{D_2} values were reported for H_2 addition to MnO_4^-.[11]

Scheme 5. Possible Mechanisms of H_2 Addition to $OsO_4(OH)^-$

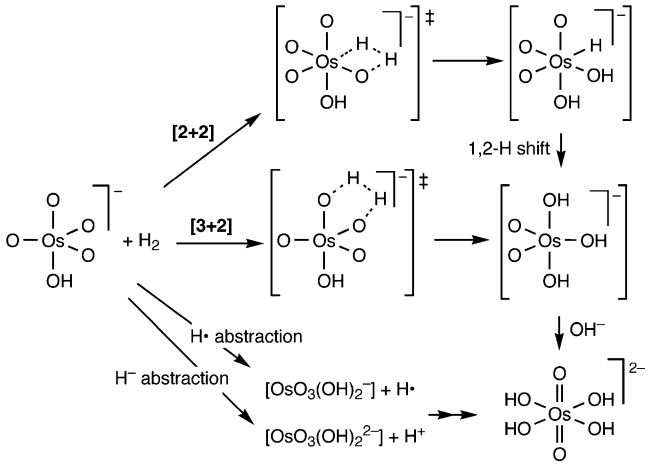

Following Halpern[10] and Collman, Strassner, et al.,[11] four mechanisms have been considered for the H_2 activation, as illustrated for $OsO_4(OH)^-$ in Scheme 5. H_2 could transfer H• or H^- to the Os^{VIII} oxidant, forming Os^{VII} + H• or $Os^{VI} + H^+$, respectively (the bottom two paths of Scheme 5). [2+2] addition could form an osmium(VIII) hydroxo-hydrido complex, Os(O)$_3$(H)(OH)(L), which might then undergo a 1,2-hydride shift to form Os(O)$_2$(OH)$_2$(L), the direct product of [3+2] addition.

Initial H• transfer is unlikely because of the thermochemistry of this step, following (in essence) an argument made by Halpern for permanganate reactions in 1957.[10] The H−H bond of 104 kcal mol^{-1} is much stronger than the O−H bond formed by the Os^{VIII} species (49−80 kcal mol^{-1}). H-atom transfer from H_2 is thus endothermic by >24 kcal mol^{-1}, a much larger value than the observed $\Delta H^‡$ of 13 kcal mol^{-1}.

(29) Different conformations of the [3+2] product were located, corresponding to the orientation of the H atoms in the two formed hydroxyl groups. The initially formed less stable conformers have H(1)−O(1)−Os−O(4) = 0° and H(2)−O(4)−Os−O(1) = 0° (see Figure 8 for labeling) and are all ΔE = 5.6−7.2 kcal mol^{-1} higher in energy than the more stable conformers. Because attempted optimization of the less stable conformer of $Os(O)_2(OH)_3^-$ was not successful, the energies of that conformer are obtained from partial optimization with the constraint of the H(1)−Os−O(4)−H(2) as 0.0°.

(30) (a) $G°[H_2\ (g) \rightarrow 2H^•\ (aq)] = G°[H_2\ (g) \rightarrow 2H^•\ (g)] + 2G°[H^•\ (g) \rightarrow H^•\ (aq)]$ = 97.2 kcal mol^{-1} [30b] + 2(2.3 kcal mol^{-1})[30d] = 101.8 kcal mol^{-1} [standard states: 1 atm pressure, 1 M H• (aq)]. (b) $G°[H_2\ (g) \rightarrow 2H^•\ (g)] = H°[H_2\ (g) \rightarrow 2H^•\ (g)] - TS°[H_2\ (g) \rightarrow 2H^•\ (g)]$ = 104.2 − 298[2(0.02742) − 0.03123] = 97.2 kcal mol^{-1}.[30c] (c) NIST Chemistry Webbook, March, 2003 Release: http://webbook.nist.gov/chemistry/. (d) Roduner, E. *Radiat. Phys. Chem.* **2005**, *72*, 201−206. (e) A value of 105.6 kcal mol^{-1} is obtained from the $E°(H^+/H^•)$ = −2.29 V vs NHE reported in: Parker, V. D. *J. Am. Chem. Soc.* **1992**, *114*, 7458 and Parker, V. D. *J. Am. Chem. Soc.* **1993**, *115*, 1201.

(31) "$[Os^{VII}O_3(OH)_3]^{2-}$" is not observed in alkaline mixtures of $Os^{VIII}O_4(OH)_n^{n-}$ and $Os^{VI}O_2(OH)_4^{2-}$.

(32) The BDE can be estimated from the BDFE using $TS(H^•, aq)$ = 1 kcal mol^{-1},[32a] and assuming (as is common[32b]) that the entropies of $OsO_4(OH)_2^{2-}$ (aq) and $[OsO_3(OH)_3^{2-}]$ (aq) are equal. This yields BDE(2)[$OsO_3(OH)_2$-(O−H)]$^{2-}$ < 65 kcal mol^{-1}. This value is consistent with rough estimates of the enthalpy for addition of H• to OsO_4, based on the low $Os^{VIII/VII}$ redox potential of +0.103 V vs SCE in CH_2Cl_2[32c] and the expected low basicity of OsO_4^- (resembling ReO_4^- and ClO_4^- in its charge and size). (a) $TS°[H^•(aq)] = T\{S°[H^•(g)] + \Delta S_{solv}°(H^•)\}$ = 298 K{(6.6[30c] − ~10[30d]) cal mol^{-1} K^{-1}} = 1 kcal mol^{-1}. (b) Mayer, J. M. In *Biomimetic Oxidations Catalyzed by Transition Metal Complexes*; Meunier, B., Ed.; Imperial College Press: London, 2000; Chapter 1 and references therein. See, however: Mader, E. A.; Larsen, A. S.; Mayer, J. M. *J. Am. Chem. Soc.* **2004**, *126*, 8066−8067. (c) Bilger, E.; Pebler, J.; Weber, R.; Dehnicke, K. *Z. Naturforsch., B: Chem. Sci.* **1984**, *39B*, 259.

(33) The electronic origin of the dramatic effect of ligands on the OsO−H BDEs and other thermochemical and kinetic properties in this system is under active investigation, and the results of this study will be reported in due course.

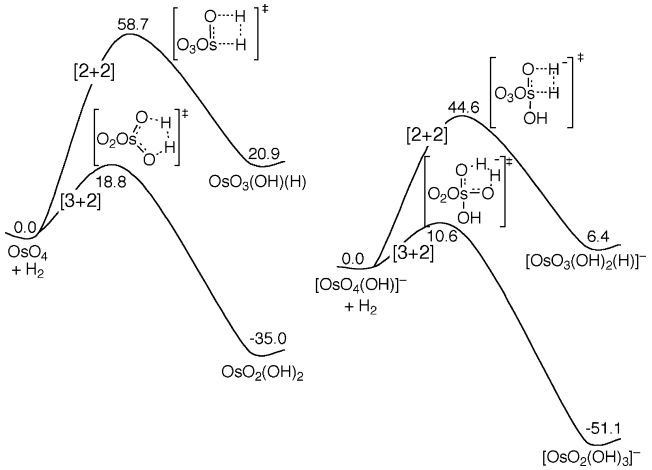

Figure 7. Calculated enthalpies (kcal mol^{-1}) at 298 K for H_2 addition to OsO_4 and $OsO_4(OH)^-$ by [2+2] and [3+2] mechanisms.

Initial hydride transfer to give $OsO_3(OH)(L)^-$ and "H^+" is also unlikely because H_2 addition proceeds at comparable rates in polar and nonpolar solvents. While a direct comparison of the same reactant in solvents of different polarity has not been possible, OsO_4·py is reduced by H_2 just as rapidly in $CHCl_3$ or *n*-hexane as $OsO_4(OH)_n^{n-}$ species are reduced in water. A hydride transfer rate-determining step should be marked by a faster rate in polar solvents because of the charge separation in the transition state. Also, H^- transfer should show a base or buffer dependence because a proton would be liberated, but this dependence is not observed.

The [2+2] and [3+2] mechanisms are difficult to distinguish experimentally, as shown by the years of controversy about the pathway for alkene additions to $OsO_4(L)_n$.[23,34] The issue for alkene oxidations has been settled in favor of the [3+2] mechanism by quantum chemical calculations,[13] particularly because the secondary isotope effects predicted by the calculations for this mechanism were confirmed by experiments.[13a]

We have used DFT calculations to locate gas-phase transition structures for addition of H_2 to OsO_4, $OsO_4(OH)^-$, and $OsO_4(NH_3)$, for both [2+2] and [3+2] pathways. The energies, enthalpies, and free energies are given in Table 2, and the enthalpic changes for OsO_4 and $OsO_4(OH)^-$ are illustrated in Figure 7. In all three cases, the [2+2] pathway is predicted to be much less favorable than the [3+2] pathway, both kinetically and thermodynamically. For instance, [3+2] addition of H_2 to OsO_4 is calculated to have a barrier of 18.8 kcal mol^{-1} and to be exothermic by -35.0 kcal mol^{-1}, while [2+2] addition to form $Os(O)_3(H)(OH)$ is calculated to have $\Delta H^{\ddagger} = 58.7$ kcal mol^{-1} and $\Delta H^{\circ} = +20.9$ kcal/mol. It should be noted that the energies for the [3+2] products in the tables and figures are for their most stable conformations, with the O−H bonds in a "head-to-tail" orientation (Figure 8). The initially formed "head-to-head" conformers are higher in energy by $\Delta E = 5.6-7.2$ kcal mol^{-1}.[29]

The calculated [3+2] gas-phase barrier of $\Delta H^{\ddagger} = 18.8$ kcal mol^{-1} for $H_2 + OsO_4$ is larger than the experimental value of $\Delta H^{\ddagger} = 13.2(2)$ kcal mol^{-1}, possibly due to the effect of solvent (see below). Better agreement is found for the reaction of H_2 with $OsO_4(OH)^-$: $\Delta H^{\ddagger} = 10.6$ kcal mol^{-1} (calculated, gas phase) versus 12.8 kcal mol^{-1} (experimental, aqueous). Computational results similar to ours for OsO_4 were obtained by Strassner et al. for H_2 addition to permanganate: The [3+2] pathway was computed to be favored over the [2+2] pathway by 46.5 kcal mol^{-1} in $\Delta H^{\ddagger}$ and 78.1 kcal mol^{-1} in ΔH°.[11]

The calculated [3+2] transition structures for H_2 addition to OsO_4 and $OsO_4(OH)^-$ (Figure 8) show concurrent stretching of H−H and Os−O bonds and formation of O−H bonds. The transition structure for $H_2 + OsO_4(OH)^-$ has the shorter H−H distance, consistent with this more exoergic reaction having an earlier transition state. The transition structure for $H_2 + OsO_4$ has C_{2v} symmetry, with equal O--H distances, but that for $H_2 + OsO_4(OH)^-$ is surprisingly asymmetric, with more than 0.1 Å difference in the length of the forming O−H bonds. The axial

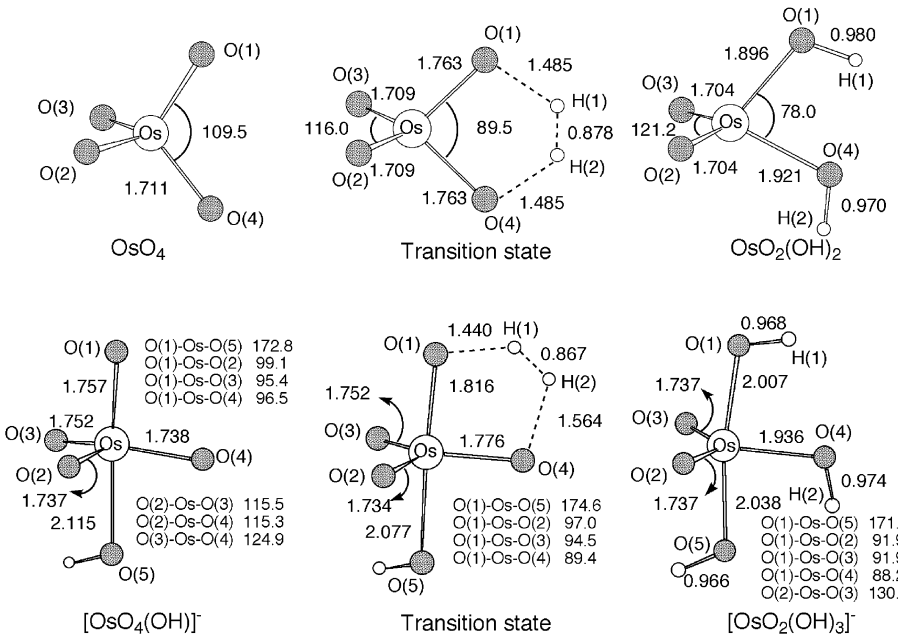

Figure 8. Calculated structures for reactants, transition states, and products for H_2 addition to OsO_4 (top) and $OsO_4(OH)^-$ (bottom) by [3+2] mechanisms. Bond lengths are given in angstroms, and bond angles are in degrees. Only the most stable conformers of $OsO_2(OH)_2$ and $OsO_2(OH)_3^-$ are shown.

oxygen, which has a longer bond to Os than the equatorial oxygen, has the shorter forming O−H bond in the transition structure.

The very large preference for the [3+2] over the [2+2] mechanism for H_2 addition is due to the [3+2] pathway being both more exoergic and also symmetry-allowed. Orbital symmetry arguments have been advanced to explain the low barriers for [3+2] alkene addition to OsO_4.[13c] The frontier orbitals of H_2 and ethylene are isolobal, so the orbital symmetry arguments are the same for H_2 addition to OsO_4.

The cyclic [3+2] pathway for addition of H_2 to OsO_4 is consistent with the small primary kinetic isotope effects observed, $k_{H_2}/k_{D_2} = 3.1$ and 3.6 for OsO_4 and $OsO_4(OH)^-$. These values are much smaller than the semiclassical maximum of $k_{H_2}/k_{D_2} = 20$ for breaking an H−H bond.[35,36] The DFT calculations give $k_{H_2}/k_{D_2} = 1.3$ for H_2/D_2 addition to OsO_4 and $k_{H_2}/k_{D_2} = 1.5$ for $OsO_4(OH)^-$.[37] To the extent that tunneling contributes to the measured reaction rate, our calculations, which do not include tunneling, should underestimate the size of the primary kinetic isotope effect.

III. Ligand Acceleration. Acceleration of the reaction of H_2 with OsO_4 by added ligands is observed experimentally and also predicted computationally. OsO_4 is unreactive with 1 atm of H_2 in chloroform or hexane at room temperature in the absence of a ligand, but reacts with a half-life of 7 h in the presence of pyridine or 1,10-phenanthroline. The effect is less pronounced in aqueous solutions, where a difference of only a factor of 3 in rate constant is observed between OsO_4 and $OsO_4(OH)^-$.[38] Ligand acceleration is also a key feature of the OsO_4-catalyzed dihydroxylation of alkenes, with rate accelerations varying from modest (×3) to dramatic (×1000) depending on the ligand and the alkene.[14a,39] Acceleration of these reactions by added ligands is surprising, because OsO_4 is electron-deficient and is reduced by H_2 and alkenes. Therefore, binding of a donor ligand might have been expected to slow both reactions rather than accelerate them.[33] The observation of this surprising effect in our study is a notable parallel between the additions of H_2 and alkenes to OsO_4 and provides indirect support for a common [3+2] mechanism.

Our DFT calculations find that the activation enthalpies for H_2 addition to $OsO_4(OH)^-$ and $OsO_4(NH_3)$ are lower than that for $H_2 + OsO_4$ by 8.2 and 3.9 kcal mol^{-1}, and the reactions of ligated OsO_4 are computed to be more exothermic by 16.1 and 10.3 kcal mol^{-1}, respectively. The calculated stabilization of the transition state is 51% of the increased $\Delta H°$ for $OsO_4(OH)^-$ and 38% for $OsO_4(NH_3)$ ($\Delta\Delta H^‡/\Delta\Delta H° = 0.51, 0.38$). The greater exothermicity implies that the ligand binds more tightly to the $Os^{VI}O_2(OH)_2$ product than to the OsO_4 reactant. Stronger ligand binding is indeed evident by the substantial shortening in the calculated Os−L bond distances in going from OsO_4L to $OsO_2(OH)_2L$: $d(Os-OH) = 2.115$ Å in $OsO_4(OH)^-$ versus 2.038 Å in $OsO_2(OH)_3^-$; $d(Os-NH_3) = 2.534$ Å in $OsO_4(NH_3)$ versus 2.253 Å in $OsO_2(OH)_2(NH_3)$. This shortening of the Os−L bonds is due, at least in part, to preference of Os^{VI} (and d^2-dioxo compounds in general[40]) to adopt octahedral structures, whereas OsO_4 binds ligands only weakly due to steric crowding and the trans effect of the oxo groups.[41] However, a detailed quantum mechanical understanding of the rate acceleration of OsO_4 addition reactions by ligands is certainly desirable.[33]

Experimentally, H_2 addition to aqueous $OsO_4(OH)^-$ is faster than that to aqueous OsO_4, but $\Delta\Delta H^‡$ is only −0.4(3) kcal mol^{-1}, not the 8.2 kcal mol^{-1} predicted for the gas-phase reaction.[38] To explore the effects of solvent on the reactions, polarized continuum model (PCM) calculations,[42] based on the gas-phase optimized structures, were performed for CCl_4 ($\epsilon = 2.23$) and H_2O ($\epsilon = 78.39$). The activation barrier for [3+2] addition of H_2 to OsO_4 was computed to be 1.4 kcal mol^{-1} lower in CCl_4 and 3.7 kcal mol^{-1} lower in water than in the gas phase. Similar solvent effects were calculated for the amine complex $OsO_4(NH_3)$. For $OsO_4(OH)^-$, the calculated solvent effects were smaller: $\Delta\Delta H^‡$ (kcal mol^{-1}) = −1.4 (CCl_4), −1.8 (H_2O). The decreased effect of aqueous solvation on $\Delta H^‡$ predicted for $OsO_4(OH)^-$, as compared to OsO_4, is due to the smaller change in polarity of the anionic complex on adding H_2. Thus, including PCM solvation reduces the difference in barriers between OsO_4 and $OsO_4(OH)^-$ from 8.2 to 6.3 kcal mol^{-1}, closer to but still substantially larger than the experimental difference of less than 1 kcal mol^{-1}. It seems likely that the aqueous solvent stabilizes the transition state for H_2 addition by more than the dielectric effect modeled in the calculations, perhaps by a specific hydrogen-bonding interaction or by coordination of a water molecule in the transition state.[38]

Conclusions

Dihydrogen readily reduces OsO_4, $OsO_4(OH)^-$, and $OsO_4(OH)_2^{2-}$ in aqueous solutions, and OsO_4(py) and OsO_4(phen) in organic solvents. The reactions require a few hours at 25 °C under 1 atm H_2. In contrast, OsO_4 in noncoordinating solvents and in the absence of a ligand is unreactive with H_2 at ambient temperatures. In aqueous solutions, larger rate constants are found for the hydroxide-bound species: $k_{OsO_4} < k_{OsO_4(OH)^-} < k_{OsO_4(OH)_2^{2-}}$. This ligand acceleration has been previously observed in the dihydroxylation of alkenes by $OsO_4(L)_n$ and exploited in enantioselective catalysis.[23]

(34) (a) Corey, E. J.; Noe, M. C. *J. Am. Chem. Soc.* **1996**, *118*, 11038. (b) Corey, E. J.; Noe, M. C. *J. Am. Chem. Soc.* **1996**, *118*, 319.
(35) (a) Taking the difference in zero-point energies between H_2 and D_2 of 625 cm^{-1} (Karplus, M.; Porter, R. N. *Atoms and Molecules*; W. A. Benjamin: Menlo Park, CA, 1971; pp 476−483) as $\Delta\Delta G^‡$, k_{H_2}/k_{D_2} would equal 20 at 298 K. (b) Weston, R. E. *Science* **1967**, *158*, 332. (c) Persky, A.; Klein, F. S. *J. Chem. Phys.* **1966**, *44*, 3617.
(36) Oxidative addition of H_2 to metal complexes, such as Vaska-type complexes, shows even lower KIE values (1.1−1.9). Faraj, A.-H.; Goldman, A. S.; Krogh-Jespersen, K. *J. Phys. Chem.* **1993**, *97*, 5890.
(37) Although H_2 has a very high stretching frequency, the transition state and products each have a total of six vibrational modes that involve hydrogen motions. As a result, based solely on zero-point energy changes, inverse kinetic and equilibrium isotope effects would be predicted. However, due to the larger translational and rotational entropy of D_2 versus H_2, normal kinetic isotope effects are predicted. Nevertheless, large inverse equilibrium isotope effects of $K_{H_2}/K_{D_2} = 0.1$ are still calculated for the reactions of both OsO_4 and $OsO_4(OH)^-$.
(38) It is possible that the OsO_4 reactions at lower pH involve coordination of a water molecule in the transition state, although the gas-phase calculations do not suggest a strong acceleration by a water ligand. The optical spectra indicate that OsO_4 is the predominant form in solution, and the calculations indicate that H_2O binds very weakly to OsO_4 in the gas phase.
(39) Criegee, R.; Marahand, B.; Wannowius, H. *Justus Liebigs Ann. Chem.* **1942**, *550*, 99.
(40) Nugent, W. A.; Mayer, J. M. *Metal−Ligand Multiple Bonds*; Wiley-Interscience: New York, 1988.
(41) Griffith, W. P. Osmium. In *Comprehensive Coordination Chemistry*; Wilkinson, G., Ed.; Pergamon: New York, 1987; Vol. 4, pp 519−633.
(42) (a) Cossi, M.; Scalmani, G.; Rega, N.; Barone, V. *J. Chem. Phys.* **2002**, *117*, 43. (b) Cossi, M.; Barone, V.; Mennucci, B.; Tomasi, J. *Chem. Phys. Lett.* **1998**, *286*, 253. (c) Mennucci, B.; Tomasi, J. *J. Chem. Phys.* **1997**, *106*, 5151. (d) Cancès, M. T.; Mennucci, B.; Tomasi, J. *J. Chem. Phys.* **1997**, *107*, 3032.

The Os^{VIII} compounds are reduced by H_2 to Os^{VI}, for instance, to osmate, $OsO_2(OH)_4^{2-}$. In contrast, most previous studies of metal oxides with hydrogen have involved either solid reactants (ZnO) or products (e.g., MnO_2 and RuO_2 from MnO_4^- and RuO_4).[9−11] The simple stoichiometry of the $OsO_4(L) + H_2$ reactions has allowed us to obtain detailed kinetic and thermodynamic data on the aqueous reactions. The thermochemistry is defined by the aqueous electrochemistry versus the normal hydrogen electrode: $\Delta G°$ varies from −20 to −27 kcal mol^{-1} depending on the pH. Kinetic studies of the aqueous reactions show primary kinetic isotope effects, $k_{H_2}/k_{D_2} = 3.1(3)$ for OsO_4 and 3.6(4) for $OsO_4(OH)^-$, implicating H−H bond cleavage in the rate-determining steps. Both reactions have low enthalpic barriers, with $\Delta H^‡ = \sim$13 kcal mol^{-1} and $\Delta S^‡ = \sim -22$ cal mol^{-1} K^{-1}.

DFT calculations show that the H_2 additions to OsO_4, both unligated and ligated, occur by a concerted [3+2] mechanism. The [3+2] addition of H_2 is computed to be highly favored over a competing [2+2] pathway. The products of the [3+2] addition reactions are calculated to be much lower in energy than those from the [2+2] addition reactions, and this energetic difference is reflected in the reaction barriers computed for the two pathways. This conclusion follows that reached by Collman, Strassner, et al. for H_2 reductions of MnO_4^- and RuO_4.[11]

The reaction of H_2 with OsO_4 is isolobal with the well-studied alkene dihydroxylation by OsO_4. The latter reaction is known to occur by a [3+2] mechanism and, like the H_2 reactions, also exhibits ligand acceleration.[13] The [3+2] mechanism for H_2 addition to OsO_4, RuO_4, and MnO_4^- is unusual for H_2 activation by a metal complex because this pathway does not involve direct binding between the metal and hydrogen. The ability of OsO_4(L) to oxidize C−H bonds, apparently by a similar [3+2] mechanism, will be described elsewhere.[43]

Experimental and Computational Methodology

Materials. Deionized water was passed through ultra-free filters, purchased from Millipore Corp. (Bedford, MA). Chloroform, *n*-hexane, benzene, methylene chloride, and pyridine were degassed and dried according to standard procedures.[44] OsO_4 (Strem, 99.95%), $K_2OsO_2(OH)_4$ (Strem, 99.9%), NaOH (Aldrich, 99.99%), Na_2HPO_4 (J. T. Baker, 99.94%), 1,10-phenanthroline (Aldrich, 99%), D_2O (Cambridge Isotope Laboratories, 99.9%), H_2 (Airgas Inc., 99.9%), and D_2 (Cambridge Isotope Laboratories, 99.9%) were used without further purification.

Instrumentation and Measurements. ^{1}H NMR spectra were obtained using a Bruker AV-300 spectrometer at ambient temperatures and are referenced to Me_4Si or a residual solvent peak: δ (multiplicity, coupling constant, number of protons, assignment). H_2 solubility measurements were performed on a Bruker DRX499. Temperature calibration of the NMR probe was accomplished by Van Geet's method.[45] IR spectra were obtained as KBr pellets using a Perkin-Elmer 1600 Series FTIR spectrometer at 4 cm^{-1} resolution. Electronic absorption spectra were acquired with a Hewlett-Packard 8453 diode array UV−visible spectrophotometer in purified solvents and are reported as λ/nm (ϵ/M^{-1} cm^{-1}). A Corning pH meter 430 was used for pH measurements and was calibrated using pH 4 and pH 10 buffers.

Kinetic Studies of $OsO_4(L)_n + H_2$. In a representative procedure, a 0.170 M aqueous solution of Na_2HPO_4 was adjusted to pH = 11.20 by addition of 3 M NaOH. A 10 mL volumetric flask was loaded with 0.5 mL of 10 mM OsO_4 solution and 9.5 mL of the pH = 11.20 buffer solution. (The pH was doubled-checked with a solution formed by mixing 0.5 mL of H_2O and 9.5 mL of 0.170 M buffer solution.) A sealable quartz cuvette with a Teflon stopcock was charged with 3 mL of the buffered OsO_4 solution as a control. An identical aliquot was added to another sealable quartz cuvette assembly, this one containing a 25 mL round-bottomed flask and a Teflon-coated stir bar (Figure 1B). The solution (in the flask portion of the assembly) was freeze−pump−thaw degassed three times. H_2 (1.03(5) atm) was added, the stopcock was closed, and the solution was vigorously shaken by hand. The solution was then poured into the cuvette portion of the apparatus. Both cuvettes were placed in the multicell holder of a UV−vis spectrometer thermostated at 24 °C. After 10 min of thermal equilibration, kinetic measurements were taken for 16 h. Between each measurement, the cuvette assembly was shaken vigorously to ensure good gas/liquid mixing, and the solution was poured back into the flask and stirred. The same procedure was used for monitoring the kinetics of reactions in organic solvents, except for the sample preparation. In a representative procedure, a 25 mL volumetric flask was charged with OsO_4 (10 mg, 41 mmol) and pyridine (0.50 g, 6.3 mmol) and brought up to 25 mL with $CHCl_3$ (1.6 mM OsO_4, 0.25 M py). The kinetic data were analyzed using the global analysis software package SPECFIT (Spectrum Software Associates, Marlborough, MA). The software analyzed the 220−550 nm portion of spectra over three half-lives and

(43) (a) Bales, B. C.; Brown, P.; Dehestani, A.; Mayer, J. M. *J. Am. Chem. Soc.* **2005**, *127*, http://dx.doi.org/10.1021/ja044273w. (b) Dehestani, A.; Watson, E. J.; Bales, B. C.; Lam, W. H.; Hrovat, D. A.; Davidson, E. R.; Borden, W. T.; Mayer, J. M., work in progress.
(44) Perrin, D. D.; Armarego, W. L. F. *Purification of Laboratory Chemicals*, 3rd ed.; Pergamon: New York, 1988.
(45) Van Geet, A. L. *Anal. Chem.* **1968**, *40*, 2227.
(46) Frisch, M. J.; Trucks, G. W.; Schlegel, H. B.; Scuseria, G. E.; Robb, M. A.; Cheeseman, J. R.; Zakrzewski, V. G.; Montgomery, J. A., Jr.; Stratmann, R. E.; Burant, J. C.; Dapprich, S.; Millam, J. M.; Daniels, A. D.; Kudin, K. N.; Strain, M. C.; Farkas, O.; Tomasi, J.; Barone, V.; Cossi, M.; Cammi, R.; Mennucci, B.; Pomelli, C.; Adamo, C.; Clifford, S.; Ochterski, J.; Petersson, G. A.; Ayala, P. Y.; Cui, Q.; Morokuma, K.; Malick, D. K.; Rabuck, A. D.; Raghavachari, K.; Foresman, J. B.; Cioslowski, J.; Ortiz, J. V.; Stefanov, B. B.; Liu, G.; Liashenko, A.; Piskorz, P.; Komaromi, I.; Gomperts, R.; Martin, R. L.; Fox, D. J.; Keith, T.; Al-Laham, M. A.; Peng, C. Y.; Nanayakkara, A.; Gonzalez, C.; Challacombe, M.; Gill, P. M. W.; Johnson, B.; Chen, W.; Wong, M. W.; Andres, J. L.; Gonzalez, C.; Head-Gordon, M.; Replogle, E. S.; Pople, J. A. *Gaussian 98*, revision A.7; Gaussian, Inc.: Pittsburgh, PA, 1998.
(47) (a) Lee, C.; Yang, W.; Parr, R. G. *Phys. Rev. B* **1988**, *37*, 785. (b) Becke, A. D. *J. Chem. Phys.* **1993**, *98*, 5648. (c) Stephens, P. J.; Devlin, F. J.; Chabalowski, C. F.; Frisch, M. J. *J. Phys. Chem.* **1994**, *98*, 11623.
(48) (a) Hay, P. J.; Wadt, W. R. *J. Chem. Phys.* **1985**, *82*, 270. (b) Wadt, W. R.; Hay, P. J. *J. Chem. Phys.* **1985**, *82*, 284. (c) Hay, P. J.; Wadt, W. R. *J. Chem. Phys.* **1985**, *82*, 299.
(49) Selected examples of the successful use of B3LYP/LanL2DZ for osmium compounds: (a) Torrent, M.; Sola, M.; Frenking, G. *Chem. Rev.* **2000**, *100*, 439−494. (b) Liang, B.; Andrews, L. *J. Phys. Chem. A* **2002**, *106*, 4042−4053. (c) Deubel, D. V. *J. Am. Chem. Soc.* **2004**, *126*, 996−997. (d) Gobetto, R.; Nervi, C.; Romanin, B.; Salassa, L.; Milanesio, M.; Croce, G. *Organometallics* **2003**, *22*, 4012−4019. (e) Grey, J. K.; Butler, I. S.; Reber, C. *Inorg. Chem.* **2004**, *43*, 5103−5111. (f) Ferrando-Miguel, G.; Gerard, H.; Eisenstein, O.; Caulton, K. G. *Inorg. Chem.* **2002**, *41*, 6440−6449. (g) Castarlenas, R.; Esteruelas, M. A.; Gutierrez-Puebla, E.; Jean, Y.; Lledos, A.; Martin, M.; Onate, E.; Tomas, J. *Organometallics* **2000**, *19*, 3100−3108.
(50) (a) Hehre, W. J.; Ditchfield, R.; Pople, J. A. *J. Chem. Phys.* **1972**, *56*, 2257. (b) Hariharan, P. C.; Pople, J. A. *Theor. Chim. Acta* **1973**, *28*, 213. (c) Francl, M. M.; Pietro, W. J.; Hehre, W. J.; Binkley, J. S.; Gordon, M. S.; Defrees, D. J.; Pople, J. A. *J. Chem. Phys.* **1982**, *77*, 3654. (d) Clark, T.; Chandrasekhar, J.; Spitznagel, G. W.; Schleyer, P. v. R. *J. Comput. Chem.* **1983**, *4*, 294.
(51) Frisch, M. J.; Trucks, G. W.; Schlegel, H. B; Scuseria, G. E.; Robb, M. A.; Cheeseman, J. R.; Montgomery, J. A.; Vreven, T., Jr.; Kudin, K. N.; Burant, J. C.; Millam, J. M.; Iyengar, S. S.; Tomasi, J.; Barone, V.; Mennucci, B.; Cossi, M.; Scalmani, G.; Rega, N.; Petersson, G. A.; Nakatsuji, H.; Hada, M.; Ehara, M.; Toyota, K.; Fukuda, R.; Hasegawa, J.; Ishida, M.; Nakajima, T.; Honda, Y.; Kitao, O.; Nakai, H.; Klene, M.; Li, X.; Knox, J. E.; Hratchian, H. P.; Cross, J. B.; Adamo, C.; Jaramillo, J.; Gomperts, R.; Stratmann, R. E.; Yazyev, O.; Austin, A. J.; Cammi, R.; Pomelli, C.; Ochterski, J. W.; Ayala, P. Y.; Morokuma, K.; Voth, G. A.; Salvador, P.; Dannenberg, J. J.; Zakrzewski, V. G.; Dapprich, S.; Daniels, A. D.; Strain, M. C.; Farkas, O.; Malick, D. K.; Rabuck, A. D.; Raghavachari, K.; Foresman, J. B.; Ortiz, J. V.; Cui, Q.; Baboul, A. G.; Clifford, S.; Cioslowski, J.; Stefanov, B. B.; Liu, G.; Liashenko, A.; Piskorz, P.; Komaromi, I.; Martin, R. L.; Fox, D. J.; Keith, T.; Al-Laham, M. A.; Peng, C. Y.; Nanayakkara, A.; Challacombe, M.; Gill, P. M. W.; Johnson, B.; Chen, W.; Wong, M. W.; Gonzalez, C.; Pople, J. A. *Gaussian 03*, revision B.05; Gaussian, Inc.: Pittsburgh, PA, 2003.

was given no constraints. Of the models examined, the best fits were obtained with a simple pseudo-first-order, A→B, model.

Computational Methodology. Using Gaussian 98,[46] density functional theory (DFT) at the Becke3LYP (B3LYP) level[47] was used to optimize the geometries of all the complexes. The effective core potentials (ECPs) of Hay and Wadt with a double-valence basis set (LanL2DZ)[48] were used to describe the Os atom,[49] while the 6-31+G-(d,p) basis set[50] was used for all other atoms. Vibrational frequencies were calculated for all stationary points, to verify whether each was a minimum (NIMAG = 0) or a transition state (NIMAG = 1) on the potential energy surface. The wave functions for all calculated species were checked for stability, with respect to the unrestricted (UB3LYP) wave functions. Solvent effects were taken into account by means of polarized continuum model (PCM) calculations[42] using the UFF force field option in which hydrogens have individual spheres. These calculations were performed with Gaussian 03.[51] Free energies of solvation were calculated for water ($\epsilon = 78.39$) and carbon tetrachloride ($\epsilon = 2.228$) as solvents, using the optimized geometries computed for the gas-phase species.

Acknowledgment. We are grateful to the National Science Foundation for financial support. We also thank Professor Christopher Cramer for very helpful discussions of the results of our PCM calculations and Ms. Theresa McBride for the drawing in Figure 1B.

Supporting Information Available: Kinetic, equilibrium, and computational data. This material is available free of charge via the Internet at http://pubs.acs.org.

JA043777R